© 2020. Published by The Company of Biologists Ltd.
This is an Open Access article distributed under the terms of the Creative Commons Attribution License (http://creativecommons.org/licenses/by/4.0), which permits unrestricted use, distribution and reproduction in any medium provided that the original work is properly attributed.

Hydrostatic pressure prevents chondrocyte differentiation through heterochromatin remodeling

Koichiro Maki[1-4§], Michele M. Nava[1-3,5], Clementine Villeneuve[1-3], Minki Chang[4], Katsuko S. Furukawa[4], Takashi Ushida[4] and Sara A. Wickström[1-3,5,6*]

[1]Helsinki Institute of Life Science, Biomedicum Helsinki, University of Helsinki, Finland

[2]Wihuri Research Institute, Biomedicum Helsinki, University of Helsinki, Finland

[3]Stem Cells and Metabolism Research Program, Faculty of Medicine, University of Helsinki, Finland

[4]Department of Mechanical Engineering, The University of Tokyo, Japan

[5]Max Planck Institute for Biology of Ageing, Cologne, Germany

[6]Cologne Excellence Cluster for Stress Responses in Ageing-associated diseases (CECAD), University of Cologne, Germany

§ Current address: Department of Biosystems Science, Institute for Frontier Life and Medical Sciences, Kyoto University, Kyoto, Japan.

*To whom correspondence should be addressed: sara.wickstrom@helsinki.fi

Journal of Cell Science • Accepted manuscript

JCS Advance Online Article. Posted on 11 December 2020

Abstract

Articular cartilage protects and lubricates joints for smooth motion and transmission of loads. Due to its high water content, chondrocytes within the cartilage are exposed to high levels of hydrostatic pressure, which has been shown to promote chondrocyte identity though unknown mechanisms. Here we investigate the effects of hydrostatic pressure on chondrocyte state and behavior, and discover that application of hydrostatic pressure promotes chondrocyte quiescence and prevents maturation towards the hypertrophic state. Mechanistically, hydrostatic pressure reduces H3K9me3-marked constitutive heterochromatin and concomitantly increases H3K27me3-marked facultative heterochromatin. Reduced H3K9me3 attenuates expression of pre-hypertrophic genes, replication, and transcription thereby reducing replicative stress. Conversely, promoting replicative stress by inhibition of topoisomerase II decreases Sox9 expression, suggesting that it enhances chondrocyte maturation. Our results reveal how hydrostatic pressure triggers chromatin remodeling to impact cell fate and function.

Introduction

The ends of long bones at the regions of joints are covered by a specialized connective tissue termed articular cartilage; a resilient, smooth, and elastic tissue with a low frictional coefficient that protects and lubricates joints for smooth motion and transmission of loads. Articular cartilage lacks blood vessels, lymphatics, and nerves, and despite being subject to a harsh biomechanical environment it has limited capacity for intrinsic healing and repair. In this regard, the preservation of healthy articular cartilage is of critical importance for joint function (Kobayashi and Kronenberg, 2014). Cartilage is formed through a process termed chondrogenesis, which proceeds through mesenchymal cell condensation and subsequent chondroprogenitor cell differentiation. Following chondrogenesis, the chondrocytes remain as resting, quiescent cells forming the cartilage tissue. Alternatively, chondrocytes undergo proliferation and terminal differentiation to hypertrophic chondrocytes and subsequently osteoblasts to form bone in a process termed endochondral ossification (Tsang & Cheah 2019).

In the late embryo and at early neonatal stages, the articular cartilage is a compact, highly cellular tissue with isotropic distribution of cells. During subsequent postnatal development and growth, the articular cartilage grows in thickness, the chondrocytes enlarge in size, extracellular matrix becomes abundant, and the tissue eventually acquires its zonal anisotropic organization (Kozhemyakina et al., 2015; Tsang and Cheah, 2019). The surface

Journal of Cell Science • Accepted manuscript

zone of articular cartilage is made of flat cells oriented along the main axis of movement and producing lubricating molecules. This surface zone contains the cartilage progenitor cells (Dowthwaite et al., 2004). Below the surface zone, the medial and deep zone comprise of large round chondrocytes surrounded by typical cartilage matrix and arranged in vertical rows (Kozhemyakina et al., 2015). How these sequential differentiation and cellular reorganization steps are regulated is unclear.

Cartilage is comprised of 70% - 80% water per wet weight, making it a highly hydrated tissue. The high water content is maintained by abundant proteoglycans present in the matrix. During joint loading, uniform normal stress is exerted on chondrocytes. As water is trapped within the tissue matrix, pressurization of the fluid initially supports the applied load. Eventually, fluid is expelled from the tissue, and the frictional force between the fluid and solid phases of the tissue dissipates energy from the applied load. In the joint, cartilage is typically exposed to stresses between 0.2 and 10 MPa (Schinagl et al., 1997; Urban, 1994). These stresses are translated to hydrostatic pressure (HP) due to fluid phase pressurization, as described above. Mechanical loading of cartilage has been recognized as an important contributor to chondrocyte identity, and for example bioreactors that mechanically load the tissue improve efficiency of chondrocyte differentiation from mesenchymal stem cells (Elder and Athanasiou, 2009). However, the precise mechanisms by which hydrostatic pressure enhance chondrogenesis are unclear.

Here we investigate the effects of physiological levels of HP on chondrocyte state and behavior. We discover that application of cyclic hydrostatic pressure promotes chondrocyte quiescence and a Sox9-high immature state through a reduction of H3K9me3-marked constitutive heterochromatin, with a concomitant increase in H3K27me3-marked facultative heterochromatin. This quiescent, Sox9-high state counteracts replicative stress and DNA damage. Conversely, promoting replicative stress by inhibition of topoisomerase II decreases Sox9 levels, suggesting DNA damage might enhance chondrocyte maturation. Our results reveal how hydrostatic pressure triggers chromatin remodeling to impact cell fate and function.

Results

Hydrostatic pressure promotes an immature quiescent state of chondrocytes

To study the effects of physiological levels of cyclic hydrostatic pressure (HP) on chondrocytes, we constructed a custom pressure chamber (Fig. 1A). Here, a high-performance liquid chromatography (HPLC) pump was combined with a solenoid valve and a

Journal of Cell Science • Accepted manuscript

pressure sensor to drive cyclic HP with a threshold pressure of 1 MPa. The frequency of the cyclic pressure was controlled to be 0.3 Hz by adjusting flow velocity of the HPLC pump.

To study the effect of HP on chondrocytes, we isolated primary mouse chondrocyte progenitors from femur head articular cartilage, as described in Materials and Methods. The identity of these cells was validated by morphological analyses as well as key identity gene (Mcam (Cd146), Sox9, Col2A1, Col1A1, Runx2) and protein (Sox9, Col2A1) expression (Supplementary Fig. 1A, B), using the chondrogenic cell line ATDC5 for comparison (Yao and Wang, 2013). The differentiation potential of the isolated chondrocytes into cartilage in response to insulin was also confirmed (Supplementary Fig. 1C).

To mimic physiological mechanical loading of cartilage, we sealed the chondrocyte-containing culture plates in plastic containers filled with culture medium and deposited them into stainless-steel chambers submerged in a water bath (Fig. 1A). Control cells were subjected to an identical procedure within a non-pressurized water bath. We then exposed cells to cyclic HP at 1 MPa, 0.3 Hz for 6 h and analyzed the effect on chondrocyte state. Analysis of chondrocyte progenitor and differentiation markers revealed that HP increased the protein levels of Sox9, the master regulator of chondrocyte identity (Fig. 1B-D) as well as the chondrocyte identity marker Col2A1 (Supplementary Fig. 1D) (Lefebvre et al., 2019). Also mRNA expression of the progenitor marker Mcam (Li et al., 2011) and markers for immature chondrocytes Acan and Col2A1 were increased (Fig. 1E). In contrast, the mRNA of markers for pre-hypertrophic and hypertrophic chondrocytes as well as osteogenic differentiation Pthr1, Runx2, and Col1A1, respectively (Lefebvre, 2019), were reduced upon HP (Fig. 1E), suggesting that HP prevents chondrocyte maturation towards the hypertrophic state. Interestingly, the mRNA levels of Sox9 were not altered (Fig. 1E), suggesting that its regulation occurred post-transcriptionally, as has been described before (Lefebvre, 2019; Lefebvre and Dvir-Ginzberg, 2017).

As the chondrocyte progenitor state has been associated with quiescence, whereas the hypertrophic state is characterized by increased proliferation (Li et al., 2017; Wuelling and Vortkamp, 2011), we analyzed proliferation and cycling of these cells in response to HP. Both freshly isolated non-immortalized and SV40-immortalized chondrocytes subjected to 6 h of HP showed reduced incorporation of EdU in a pulse experiment where EdU was applied at the onset of HP (Fig. 1F, G, Supplementary Fig. 1E). In addition, quantification of DNA content (DAPI intensity) as a function of EdU incorporation revealed an increase in cells in G1/G0 and a concomitant reduction in S phase (Fig. 1H). In contrast, no increase in cell death was observed, as assessed by markers of apoptosis and necrosis (Supplementary Fig. 1F, G). To further address if HP indeed evoked quiescence or only slowed down replication,

Journal of Cell Science • Accepted manuscript

we analyzed levels of transcriptional elongation (RNA polymerase II phosphorylated at Serine 2; RNAPII-S2P) and observed decreased levels of transcription upon HP (Fig. 1I, J; Supplementary Fig. 1H). Further, the Sox9-regulated cell cycle inhibitor and stem cell quiescence gene P21 (Panda et al., 2001) was strongly upregulated in response to HP (Fig. 1K). In contrast, P27 and P16, other markers for quiescence/senescence (Diekman et al., 2018; Miller et al., 2007; Zhao et al., 2016), were not induced (Fig. 1K), indicative of a response specific to P21. Collectively these results indicated that cyclic, physiological levels of HP induced chondrocyte quiescence and promoted the progenitor state.

Hydrostatic pressure triggers nuclear shrinkage and heterochromatin remodeling

To understand how HP regulates chondrocyte identity and state, we sought to identify immediate cellular effects of HP. To this end we established a unique experimental setup to facilitate live imaging of cells under HP (Fig. 2A). Here, ATDC5 chondrocytes were seeded on a transparent, rigid sapphire glass substrate to minimize focus change induced by substrate deformation upon HP. The sapphire substrate was placed in a stainless-steel chamber and chondrocytes stained with Hoechst 33342 to visualize nuclei were exposed to constant HP of 10 MPa under live imaging. The most obvious immediate response to HP was the decrease in nuclear size, which occurred within minutes of HP application (Fig. 2B, Supplementary Movies 1 and 2). Decreased nuclear area and volume were confirmed by immunofluorescence analyses of fixed mouse chondrocytes (Fig. 2C). Interestingly, no significant alterations in nuclear circularity were observed (Supplementary Fig. 2A). Although, as expected, nuclear volume was influenced by cell cycle (Neumann and Nurse, 2007), the HP-induced decrease in nuclear size was independent of EdU incorporation (Supplementary Fig. 2B), suggesting that the effect of HP on replication/quiescence did not explain the reduced nuclear volume.

To understand the mechanisms of the nuclear volume decrease we analyzed the nuclear lamina and heterochromatin, which both play important roles in the regulation of nuclear shape and mechanics (Kirby and Lammerding, 2018; Miroshnikova et al., 2017). Lamin A/C levels were not significantly altered in response to HP (Supplementary Fig. 2C), consistent with previous studies showing that Lamin A levels scale with tensile stiffness (Swift et al., 2013) rather than bulk compression as applied here. In contrast, we observed that the levels of constitutive, H3K9me3-marked heterochromatin were reduced (Fig. 2D, E, Supplementary Fig. 2D). This reduction was particularly evident at the nuclear periphery, proximal to the lamina (Fig. 2F). In contrast, facultative heterochromatin marked by H3K27me3 was found increased upon HP (Fig. 2G, H, Supplementary Fig. 2E). As H3K9me3-marked

Journal of Cell Science • Accepted manuscript

heterochromatin is considered more compacted than H3K27me3, we hypothesized that the net effect of this HP-induced chromatin remodeling would be chromatin decompaction. Indeed, analysis of bulk chromatin accessibility using micrococcal nuclease (MNase) digestion revealed a small but reproducible increase in chromatin accessibility to MNase (Supplementary Fig. 2F). Interestingly, the HP-induced changes in nuclear size, H3K9me3 heterochromatin and EdU incorporation were restored to steady state within 3h after halting pressurization, suggesting that the responses are reversible (Fig. 2I), similar to what has been described for osmotic stress (Irianto et al., 2013). Together these data indicated that HP triggered reversible nuclear shrinkage and reduction in H3K9me3 particularly at the nuclear periphery with a parallel increase in H3K27me3.

H3K9me3 heterochromatin regulates chondrocyte quiescence and identity

To understand if the observed decrease in H3K9me3 and increase in H3K27me3 would contribute to the effects of HP on chondrocyte state, we depleted the methyltransferases responsible for catalyzing these histone modifications using siRNA. Depletion of the H3K9me3 methyltransferase Suv39H1 led to an expected decrease in H3K9me3 levels (Fig. 3A). As reported previously in other cell types (Cooper et al., 2014; Le et al., 2016; Peters et al., 2003), the decrease in H3K9me3 was accompanied by an increase in H3K27me3 (Fig. 3B, C). Interestingly, depletion of Suv39H1 and subsequent reduced H3K9me3 was sufficient to trigger a decrease in nuclear volume without affecting circularity (Fig. 3D), a similar morphological change in the nucleus that was observed in response to HP. Suv39H1 depletion also resulted in increased Sox9 protein expression (Fig. 3E). Similarly to HP, Sox9 mRNA was not significantly altered, whereas Mcam and to a lesser extent Acan, were slightly increased. More prominently, markers for hypertrophic maturation (Pthr1, MMP13 and Col1a1) were decreased (Fig. 3F). Furthermore, we observed reduced transcriptional elongation (RNAPII-S2P) and EdU incorporation in response to Suv39H1 depletion (Fig. 3G, H). Thus, Suv39H1 depletion to a large extent phenocopied the effects of HP on chondrocytes, attenuating maturation towards the hypertrophic chondrocyte state while decreasing nuclear volume, replication and transcription.

Depletion of the H3K27me3 methyltransferase Ezh2 led to a strong decrease in H3K27me3, as expected, but also to an increase in H3K9me3 (Supplementary Fig. 3A-C). Interestingly, Ezh2 depletion triggered an increase in nuclear volume (Supplementary Fig. 3D), further suggesting that heterochromatin is capable of modulating nuclear volume. However, in contrast to depletion of Suv39H1, depletion of Ezh2 and the accompanying decrease in H3K27me3 and mild increase in H3K9me3 did not impact Sox9 expression, EdU

Journal of Cell Science • Accepted manuscript

incorporation, or transcription (Supplementary Fig. 3E, F). Collectively, these experiments suggested that reduced H3K9me3 was responsible for the effects of HP on chondrocyte identity, decreased replication and transcription, whereas increased H3K27me3 might represent a compensatory effect with a possible role in nuclear volume regulation.

Hydrostatic pressure-controlled chondrocyte quiescence prevents DNA damage

Next, we aimed to understand the functional relationship between the various effects of HP on DNA metabolism: reduction in H3K9me3 and slight chromatin decompaction, and the coordinated decrease in replication and transcription. The common denominator of these three phenomena is their effect in reducing barriers for transcription and transcription-replication conflicts that lead to replication fork stalling and genomic instability (García-Muse and Aguilera, 2016). As stalled replication forks are sensed by the DNA damage machinery, we thus sought to examine DNA damage and its relationship with replication upon exposure to HP. Immunofluorescence analyses revealed significantly reduced γH2AX in chondrocytes exposed to HP (Fig. 4A, B), whereas control cells showed frequent pan-nuclear staining of γH2AX as an indication of replicative stress (Fig. 4A, B and Supplementary Fig. 4A, B) (Toledo et al., 2011). Alleviated DNA damage under HP was further verified with alkaline comet assay (Fig. 4C). γH2AX was particularly high in cells with high EdU incorporation, confirming the relationship between replication and DNA damage (Fig. 4A, D). However, the positive correlation between EdU and γH2AX remained comparable in HP and control cells (Fig. 4D), suggesting that reduced γH2AX upon HP was secondary to reduced replication and transcription, with less opportunity to fork collision. Similarly to the responses in nuclear volume, H3K9me3 and EdU incorporation, γH2AX was also restored 3h after halting pressurization (Fig. 4E).

To test if exposure to HP indeed reduced generation of DNA damage and did not enhance repair, we induced replicative stress and DNA damage by inhibiting topoisomerase II using etoposide as a short pulse (1 h) (Smart et al., 2008), and after washing out etoposide exposed cells to HP (Fig. 4F). Interestingly, no difference was observed between control and HP on the rate of recovery after DNA damage (Fig. 4G, H), confirming that the initial differences in γH2AX were due to less amount of damage generated.

To probe the relationship between H3K9me3 and DNA damage, we depleted Suv39H1 and quantified γH2AX intensity. As predicted, Suv39H1-depleted cells displayed lower levels of γH2AX (Fig. 4I). Furthermore, overexpression of Suv39H1-IRES-GFP to prevent decreased H3K9me3 upon HP, also prevented HP from reducing DNA damage (Fig. 4J). Interestingly, Suv39H1 overexpression alone decreased both γH2AX levels (Fig. 4J) and EdU

Journal of Cell Science • Accepted manuscript

incorporation (Supplementary Fig. 4C), indicating that H3K9me3 levels have a biphasic effect on replication, where both very high (Suv39H1 overexpression) and very low (Suv39H1 depletion) H3K9me3 levels reduce replication and thereby most likely replication stress. Collectively, these data showed that H3K9me3 levels impacted replication rates in chondrocytes and that HP-induced chromatin decompaction protected cells against replication stress and DNA damage.

Loss of quiescence induces replicative stress to promote loss of chondrocyte progenitor state

To dissect the relationship between quiescence, DNA damage and Sox9 expression, we asked if decreasing replication could reduce replicative stress and thus DNA damage. Promoting quiescence by serum starvation reduced both EdU incorporation as well as γH2AX intensity (Fig. 5A, B). Serum starvation also increased Sox9 expression (Fig. 5C), suggesting that reduced replication might control chondrocyte state. Importantly, a similar correlation was observed in the articular cartilage *in vivo* in postnatal day 2 (P2) mouse cartilage, where the Sox9-positive progenitor cells at the surface zone showed low rates of cycling as defined by Ki67 as well as no γH2AX signal (Fig 5D, E). In contrast, deeper into the medial zone, the cells had lower Sox9 expression, as expected, and showed higher frequency of Ki67-positive actively cycling cells, which correlated with γH2AX signal (Fig. 5D, E). Interestingly, and as expected based on high levels of HP, H3K9me3 intensity was lower at the surface zone whereas, deeper into the medial zone, cells showed a higher H3K9me3 intensity, suggesting that physiological stresses *in vivo* in P2 mouse cartilage might trigger heterochromatin changes (Fig. 5F). The levels of H3K27me3 did not, however, substantially differ between the surface and medial zone of the P2 cartilage, indicative of more complex regulation of this histone in vivo compared to cultured chondrocytes (Supplementary Fig. S5A).

Finally, we asked if replicative stress/DNA damage could promote chondrocyte differentiation. To this end we induced DNA damage by inhibiting topoisomerase II using etoposide. Intriguingly, etoposide decreased Sox9 expression in a dose-dependent manner (Fig. 5G, H), suggestive of differentiation.

Taken together, these experiments showed that quiescence associated with the progenitor state of chondrocytes reduces replication stress, whereas promotion of replication stress might trigger chondrocyte differentiation.

Journal of Cell Science • Accepted manuscript

Discussion

Our study demonstrates how hydrostatic pressure regulates chromatin architecture and replication to control chondrocyte differentiation. We observe that cyclic HP mimicking physiological loading of the articular cartilage leads to decreased nuclear volume, chromatin decompaction, and promotion of a quiescent, less mature chondrocyte state, similar to what is found in vivo on the surface zone of the articular cartilage.

The observed HP-triggered decrease in nuclear volume is consistent with previous reports where chondrocytes have been subjected to compression and hyperosmotic pressure (Guilak, 1995; Irianto et al., 2013). As in this previous work, the decrease in nuclear volume is an immediate response to HP and is independent of the cell cycle. The decrease in nuclear volume concomitant with chromatin decompaction, however, is somewhat surprising, given that chromatin decompaction is reported to increase nuclear volume by entropic pressure (Mazumder et al., 2008). While this concept is intriguing, it is also reasonable to postulate that the volume changes resulting from chromatin decompaction could be buffered by deformation of nucleocytoplasmic components, water exchange through nuclear pores, or other more complex mechanisms. It is also important to consider that HP decreases H3K9me3 particularly at the nuclear lamina, which perturbs the attachment of chromatin to nuclear lamina (Bondarenko et al., 2017; Towbin et al., 2012), whereas H3K27me3 heterochromatin which is not anchored to the lamina is increased. The specific reduction of H3K9me3 at the nuclear periphery might attenuate nuclear membrane tension (Enyedi and Niethammer, 2017; Nava et al., 2020), resulting in decreased volume. As the roles of forces in nuclear volume regulation are not well understood, this aspect remains open for further investigation.

We further observe that HP attenuates maturation of chondrocytes towards a hypertrophic state, characterized by increased expression of immature chondrocyte/progenitor markers Sox9, Acan, Col2A1 and Mcam, and decreased expression of pre-hypertrophic and osteogenic state markers Ptrh1, Runx2 and Col1A1. Effects of hydrostatic pressure on chondrocytes have been investigated at various magnitudes, application times and frequencies of cyclic HP. Consistent with our observations, physiological levels of HP (up to 10 MPa) have been reported to increase expression levels of Sox9, Col2A1and GAG in mesenchymal stem cells and cartilage progenitors (Li et al., 2016; Miyanishi et al., 2006), while extreme levels of HP (25 MPa) seem to decrease Col2A1 and Acan expression in a chondrocytic cell line (Montagne et al., 2017). Collectively this implies that there might be a

Journal of Cell Science • Accepted manuscript

mechanical threshold in chondrocytes, which determines the effect on differentiation. Alternatively, as all the studies use different cell culture models, some of the effects might be cell type specific. More direct comparisons with varying HP amplitudes and frequencies are required to understand how chondrocytes respond to HP under physiological and pathological stress.

We further observe that inducing replication stress decreases Sox9 expression, indicative of increased chondrocyte differentiation. This is consistent with *in vitro* studies of a chondrocytic cell line, where chondrocyte differentiation is associated with increased replication stress (Spaapen et al., 2013). The precise mechanisms by which replication stress could regulate chondrocyte differentiation is unclear. Interestingly, Sox9 has been shown to be targeted for proteasomal degradation upon DNA damage (Hong et al., 2016), and it will be interesting to study if similar mechanisms operate upon physiological levels of replication stress.

Parallel to the effects on cell state, we observe a wide-spread reduction in H3K9me3 heterochromatin upon HP, which limits replication and thus replication stress in the chondrocytes. This is consistent with the known susceptibility of heterochromatin regions to replication stress and formation of fragile sites, regions in the genome that show DNA breakage the presence of replication stress (Janssen et al., 2018). A possible explanation of this predisposition of heterochromatin to replication stress could stem from the higher repeat content of heterochromatic regions, resulting in stable secondary structures inhibitory to fork progression (Branzei and Foiani, 2010; Pearson et al., 2005; Zhao et al., 2010) that require additional mechanisms to be properly duplicated (Miller et al., 2006) While not contradictory to these observations, our studies suggest that the degree of chromatin compaction (or phase separation/mobility) could present an additional, sequence-independent factor in promoting susceptibility of heterochromatin to replication stress. This possibility is supported by findings where depleting Suv39H1 to decrease in H3K9me3 alleviates excessive DNA damage in progeroid cells and rescues DNA repair in ATM-deficiency (Goodarzi et al., 2008; Liu et al., 2013).

How HP is sensed and how its effects are transduced into the nucleus remain key open questions. As cartilage tissue and chondrocytes are reported to be incompressible under low strains (Bachrach et al., 1998; Ofek et al., 2009), a pressure-sensing mechanism in the absence of a gas–liquid interface remains unclear. One possible mechanism is a change in plasma membrane fluidity, which could activate mechanosensitive ion channels (Nirmalanandhan et al., 2015). A recent study on the endothelial cell cytoskeleton indeed showed that HP-induced cytoskeletal remodeling was mediated by mechanosensitive cation channels and subsequent elevation in intracellular Ca2+ (Prystopiuk et al., 2018).

Journal of Cell Science • Accepted manuscript

Interestingly, we recently showed that elevated intracellular Ca2+, released from the endoplasmic reticulum upon cell stretching or cell compression, mediates decreased H3K9me3 (Nava et al., 2020). In addition, intracellular Ca2+ is elevated by osmotic swelling of nuclei (Enyedi and Niethammer, 2017) Thus, Ca2+ signaling through mechanosensitive channels could be a key mediator of the cellular and nuclear effects in response to a number of stimuli that induce mechanical stress and/or osmotic changes, including stretch, compression, and HP.

Taken together we show that HP acts as a physiological stimulus on chondrocytes to regulate H3K9me3 levels, chromatin architecture and replication to maintain the progenitor state. As the progenitors localize close to the articular surface where pressure is the highest, more in depth *in vivo* studies will show if this localization is directly controlled by extrinsic force.

Methods

Isolation of murine chondrocytes

Chondrocytes were isolated from femoral heads of postnatal day 20 (P20) male C57BL/6J mice essentially as described previously (Gosset et al., 2008). Femoral heads were carefully isolated, minced and pre-digested in Dulbecco's minimal essential medium (MEM) containing 3 mg/ml Collagenase D (Roche) for 30 min. After pre-digestion, cartilage pieces were disrupted by pipetting and digested in Dulbecco's MEM containing 0.5 mg/ml Collagenase D for 1h. Cell suspension was passed through a 40 µm cell strainer and cells were plated on Mitomycin C-treated (10 µM) J2 fibroblast feeders and cultured in Dulbecco's MEM, 10% fetal bovine serum (Gibco). After 48 h of cell culture, remaining feeder cells were removed by trypsinization and cells were either used directly for experiments (labeled as non-immortalized cells) or transfected by SV40 large-T antigen for immortalization. Immortalized cells were cultured in Dulbecco's MEM, 10% FBS (Gibco). Non-immortalized cells were used for analyses of quiescence, all other experiments were carried out with immortalized cells. ATDC5 murine carcinoma-derived chondrogenic cell line was from ATCC (ECACC99072806) and was cultured in Dulbecco's MEM/Ham's F12 (1:1), 5% FBS (Gibco). ATDC5 cells were used for initial comparison with isolated mouse chondrocytes and live imaging experiments. All cell culture was performed in 5% CO_2 at 37 °C. All cells were tested negative for mycoplasma. Animals were housed and maintained according to FELASA guidelines in the animal facility of University of Helsinki. All experiments were approved by local authorities (permit number KEK-18-020).

Journal of Cell Science • Accepted manuscript

Application of cyclic hydrostatic pressure

300 000 cells (35 mm petri dish) or 30 000 cells (14 mm glass bottom dish) were seeded 24 h prior to the experiment. For pressurization, cell culture dishes were first sealed into a plastic bag filled with culture medium (Dulbecco's MEM, 10% FBS), which were deposited in a stainless steel chamber in a water bath at 37 °C. A high-performance liquid chromatography (HPLC) pump (Senshu Scientific) was used to pressurize cells. Frequency of cyclic pressure was controlled by a pressure sensor and a solenoid valve (L. Tex). The threshold of hydrostatic pressure and its frequency was set to be 1 MPa and 0.3 Hz. After hydrostatic pressure application was completed, the plastic bag was immediately opened and the cell culture dish was subjected to fixation and lysis for further analysis.

Real-time imaging of cells under HP

For real-time imaging, a sapphire glass substrate was coated with fibronectin (10 µg/ml) in phosphate-buffered saline (PBS) for 1 h at 37°C. 30 000 ATDC5 cells were seeded on fibronectin-coated sapphire glass 24 h before the experiment. Cells were treated with Hoechst 33342 for DNA staining 1h before experiment and then placed in a stainless steel chamber. A high pressure pump (Nihon Seimitsu Kagaku) was used to increase pressure in the chamber, and a relief valve was used to adjust the pressure to be 10 MPa. An epi-fluorescent microscope (IX71; Olympus) with an 30X objective and a cooled CCD (C7780-10; Hamamatsu Photonics) were used for live imaging.

Transfections, plasmids and RNAi

siRNAs targeting Suv39H1 (#1: s74606, #2: s74607; Thermo Fisher Scientific) and Ezh2 (#1: S65775, #2: S65776; Thermo Fisher Scientific), and negative control siRNA (AM4635) were from Ambion (Silencer Select). Suv39H1-IRES-EGFP was from Sino Biological (ID: 28113). Transfections were performed using Lipofectamine RNAiMax (Thermo Fisher Scientific) for siRNA, and Lipofectamine 2000 (Invitrogen) for protein expression according to manufacturers' instructions. Experiments were performed after 72 h (siRNA), or 24 h (protein expression) of transfection.

Immunofluorescence stainings

Cells were fixed in ice-cold methanol for 5 min, permeabilized with 0.3% Triton X-100 in PBS, and blocked in 5% bovine serum albumin (BSA). Samples were incubated overnight at 4 °C in primary antibody in 1% BSA/0.3% Triton X-100/PBS, followed by washing in PBS and incubation in secondary antibody in 1% BSA/0.3% Triton X-100/PBS. The following

Journal of Cell Science • Accepted manuscript

antibodies were used: H3K9me3 (Cell Signaling 13969; 1:5000), H3K27me3 (Cell Signaling 9733; 1:5000), Phospho-Histone H2A.X (Ser139) (Cell Signaling 9718; 1:5000), Phospho-Histone H2A.X (Ser139) (Merck Millipore 05-636; 1: 1000), Lamin A/C (Cell Signaling 4777; 1:5000), Sox9 (Cell Signaling 82630; 1:5000), RNAPII-S2p, (Abcam 5095; 1:5000), and Collagen 2A1 (Thermo Fisher Scientific MA5-12789; 1:5000), and Cleaved Caspase-3 (Cell Signaling 9664; 1:1000). EdU incorporation assay was performed using Click-iT™ EdU Cell Proliferation Kit (Thermo Fisher Scientific). 1 μM EdU was added to the culture medium filled in the plastic bag prior to HP and detected after fixation.

Cell viability assay

Cell viability, apoptosis and necrosis was examined with Apoptotic/Necrotic Cells Detection Kit (PK-CA707-30017; PromoKine), where apoptotic and necrotic cells were labeled with FITC-Annexin V and Ethidium Homodimer III (EthD-III), respectively. Cells were subjected to HP for 6h after which samples were subjected to analysis according to the manufacturer's instructions. The stained samples were imaged using an epifluorescent microscope.

Immunohistochemistry of cartilage

Hind legs of postanal day 2 (P2) C57Bl6 mice were fixed by 4 % PFA for 48 h at room temperature. Fixed samples were decalcified in 10% EDTA (pH 7.4) for 7 days at room temperature on a rocker, and then embedded into paraffin. 8 μm sections were cut with a microtome and deparaffinized, after which antigen retrieval in citrate buffer (pH 6.0) was performed by a microwave, Sections were blocked with 5% goat serum/3%BSA and subjected to immunofluorescence staining by using following antibodies; Phospho-Histone H2A.X (Ser139) (Cell Signaling 9718; 1:500), Sox9 (Cell Signaling 82630; 1:500), and Ki67 (Cell Signaling 9449; 1:500), H3K9me3 (Cell Signaling 13969; 1:500)., H3K27me3 (Cell Signaling 9733; 1:500),

Confocal microscopy

All fluorescence images were obtained by laser scanning confocal microscopy (SP8X; Leica) with Leica Application Suite software (LAS X version 2.0.0.14332), using 40x or 60x immersion objectives. Images were acquired at room temperature using sequential scanning of frames with a step-size of 0.5 μm, after which all planes encompassing complete cell nuclei were projected as a maximum intensity. Images were achieved with the same settings for all samples within an experiment.

Journal of Cell Science • Accepted manuscript

Image analysis

Images were analyzed using Fiji (Schindelin et al., 2012). For imaging of nuclei, fields for observation were randomly selected based on the presence of nuclei assessed by DAPI staining. Confocal stack images were first converted to maximum projection images and nuclear outlines were generated by automated thresholding for DAPI staining and mean fluorescence intensities of nuclear staining of interest were quantified within the nuclear outlines.

For the intensity analysis of periphery and central regions of nuclei, single representative confocal plane with the largest xy-cross-sectional area of nucleus was chosen from confocal stack images (DAPI channel) and the line-scanned intensity profiles for DAPI and H3K9me3 were analyzed. To quantify H3K9me3 intensity in the nuclear periphery vs center, an area of interest was generated by thresholding on maximum projections of DAPI fluorescence. The area of interest was first redirected on midplanes of H3K9me3-stained confocal stacks to quantify mean H3K9me3 intensity I_{tot} in the total nuclear area S_{tot}. The area of interest was then reduced by a factor -11 to shrink it ~2 µm from the outer edge, and the area was redirected on the midplanes of confocal stacks to quantify mean H3K9me3 intensity I_{non} in the non-peripheral area S_{non}. Finally, the peripheral H3K9me3 intensity was calculated by dividing I_{tot}-I_{non} by S_{tot}-S_{non}.

For nuclear imaging of histone modifications in the femoral articular cartilage from P2 mice, areas of interest were manually generated using the DAPI staining from the contact surface positions (30 µm) towards medial positions (30-60µm from contact surface) after which mean fluorescence intensities of nuclear stainings were quantified.

Western blotting

Cells were lysed in the RIPA buffer (150mM NaCl, 50mM Tris-HCl, 5mM EDTA, 0.1% SDS (v/v), 1% sodium deoxycholate (v/v) and 1% Triton X-100 (v/v), supplemented with proteinase inhibitor (cOmplete Mini; Roche) and phosphatase inhibitor (Phos-Stop; Pierce) cocktail tablets) at 4 °C and subjected to additional solubilization by sonication using Bioruptor II (BM Equipment Co., Ltd.) for 15 cycles at 4 °C. For histone extraction, cells were first lysed in Triton Extraction Buffer (PBS containing 0.5% Triton X-100 (v/v), proteinase inhibitor and phosphatase inhibitor) at 4 °C, from which nuclei were obtained as a precipitate after centrifugation (2,000g for 10 min at 4 °C). Nuclei were incubated overnight at 4 °C in 0.2 N HCl and solubilized histone was collected in a supernatant after centrifugation (17,000g for 10 min at 4 °C) and neutralized by adding 1.0 N NaOH.

Journal of Cell Science • Accepted manuscript

Protein concentrations were quantified with BCA (Thermo Fisher Scientific), suspended in Laemmli sample buffer and denatured. Equal amounts of protein were loaded in 10% SDS-PAGE gels. Peptides separated by SDS-PAGE was transferred to PVDF membrane using the Trans-Blot Turbo Transfer System (Biorad), and the membrane was blocked with 5% BSA or 5% Milk in TBS containing 0.2% Tween 20 (TBS-T) for 1 h at room temperature. After blocking, membranes were with primary antibodies overnight at 4 °C, washed with TBS-T and incubated with HRP-conjugated secondary antibodies for 30 min at room temperature. HRP was detected by Enhanced Chemi Luminescence (ECL) reaction and chemiluminescence images were obtained using ChemiDoc Imaging System (Biorad) Following primary antibodies were used: GAPDH (Calbiochem 1001; 1:100000), total H3 (Cell Signaling 3638; 1:10000), H3K9me3 (Cell Signaling 13969; 1:5000), H3K27me3 (Cell Signaling 9733; 1:5000), Phospho-Histone H2A.X (Ser139) (Cell Signaling 9718; 1:5000), Lamin A/C (Cell Signaling 4777; 1:5000), Sox9 (Cell Signaling 82630; 1:5000), RNAPII-S2p (Abcam 5095; 1:5000), and Collagen 2A1 (Thermo Fisher Scientific MA5-12789; 1:5000), and Cleaved Caspase-3 (Cell Signaling 9664; 1:5000).

Micrococcal nuclease assay

After pressurization or chemical treatment, cells were washed twice with ice-scold PBS and lysed in Lysis buffer (10 mM Tris-Hcl (pH 7.4), 10 mM NaCl, 3mM $MgCl_2$, 0.5% NP-40, 0.15 mM Spermine, 0.5 mM Spermidine) for 10 min on ice. Nuclei were washed with Digestion buffer (10 mM Tris-Hcl (pH 7.4), 15 mM NaCl, 60 mM KCl, 0.15 mM Spermine, 0.5 mM Spermidine) and resuspended in 1mM $CaCl_2$-containing Digestion buffer. For chromatin digestion, Micrococcal Nuclease (3 units, New England Biolabs, Inc.) was added to nuclei suspension (100k cells in 100 µl) and incubated for 15 min at 37 °C. Chromatin digestion was stopped by adding 25 µl of Stopping buffer (100mM EDTA, 10mM EGTA), followed by protein digestion in 1 mg/ml Proteinase K and 1% SDS (v/v) for overnight at 37 °C. Digested genomic DNAs were purified with NucleoSpin Tissue (Macherey-Nagel GmbH & Co. KG) and quantified with Qubit assay (Thermo Fisher Scientific). Equal amount of genomic DNAs (25 ng) for each sample was analyzed Agilent 2200 TapeStation with Genomic DNA Screen Tape (Agilent Technologies).

qPCR

RNA was isolated using the Nucleospin RNA Plus kit (Macherey&Nagel), after which cDNA was synthesized using the High-Capacity cDNA Reverse Transcription Kit (Applied Biosystems). qPCR was performed on the StepOne Plus Real Time PCR System (Applied Biosystems) using the DyNAmo ColorFlash SYBR Green Mix (Thermo Fisher). Gene

Journal of Cell Science • Accepted manuscript

expression changes were calculated following normalization to β-tubulin using the comparative Ct (cycle threshold) method. For primer sequences see Supplementary Table 1.

Statistical analyses

All experiments performed in the manuscript were repeated at least in 3 independent experiments/biological replicates. Sample size was predetermined using power analysis. No datapoints were excluded from the analyses. Statistical analyses were performed using GraphPad Prism software (GraphPad Prism 8). Statistical significance was determined by the specific tests indicated in the corresponding figure legends.

Journal of Cell Science • Accepted manuscript

Acknowledgements

We thank Yekaterina Miroshnikova for discussions, Anu M. Luoto for expert technical assistance, the Light Microscopy Unit, and the Biomedicum Helsinki Imaging Unit for imaging and image analysis support. This work was supported by the Helsinki Institute of Life Science, Wihuri Research Institute, Academy of Finland (project 317597), and Max Planck Society. KM is supported by JSPS KAKENHI Grant number 17J03032, Nakatomi Foundation, and Yamada Science Foundation. TU is supported by JSPS KAKENHI Grant Number 15H01800. MMN is supported by the ERC under the European Union's Horizon 2020 research and innovation programme (Marie Sklodowska-Curie Actions, grant agreement No. 748004 - MiMEtiC).

Author contributions

KM and MMN designed and performed most of the experiments and analyzed data. CV performed *in vivo* experiments. MC performed the live imaging experiment. KSF and TU designed experimental setups for pressurization. SAW supervised the study, designed experiments, analyzed data and wrote the paper. All authors commented and edited the manuscript.

Declaration of interests

The authors declare no conflict of interest.

Journal of Cell Science • Accepted manuscript

References

Bachrach, N. M., Mow, V. C. and Guilak, F. (1998). Incompressibility of the solid matrix of articular cartilage under high hydrostatic pressures. *J. Biomech.* **31**, 445–451.

Bondarenko, S. M., Artemov, G. N., Sharakhov, I. V and Stegniy, V. N. (2017). Tissue-specific features of the X chromosome and nucleolus spatial dynamics in a malaria mosquito, Anopheles atroparvus. *PLoS One* **12**, e0171290.

Branzei, D. and Foiani, M. (2010). Maintaining genome stability at the replication fork. *Nat. Rev. Mol. Cell Biol.* **11**, 208–219.

Cooper, S., Dienstbier, M., Hassan, R., Schermelleh, L., Sharif, J., Blackledge, N. P., De Marco, V., Elderkin, S., Koseki, H., Klose, R., et al. (2014). Targeting polycomb to pericentric heterochromatin in embryonic stem cells reveals a role for H2AK119u1 in PRC2 recruitment. *Cell Rep.* **7**, 1456–1470.

Diekman, B. O., Sessions, G. A., Collins, J. A., Knecht, A. K., Strum, S. L., Mitin, N. K., Carlson, C. S., Loeser, R. F. and Sharpless, N. E. (2018). Expression of p16INK4a is a biomarker of chondrocyte aging but does not cause osteoarthritis. *Aging Cell* **17**, e12771.

Dowthwaite, G. P., Bishop, J. C., Redman, S. N., Khan, I. M., Rooney, P., Evans, D. J. R., Haughton, L., Bayram, Z., Boyer, S., Thomson, B., et al. (2004). The surface of articular cartilage contains a progenitor cell population. *J. Cell Sci.* **117**, 889 LP – 897.

Elder, B. D. and Athanasiou, K. A. (2009). Hydrostatic pressure in articular cartilage tissue engineering: from chondrocytes to tissue regeneration. *Tissue Eng. Part B. Rev.* **15**, 43–53.

Enyedi, B. and Niethammer, P. (2017). Nuclear membrane stretch and its role in mechanotransduction. *Nucleus* **8**, 156–161.

García-Muse, T. and Aguilera, A. (2016). Transcription–replication conflicts: how they occur and how they are resolved. *Nat. Rev. Mol. Cell Biol.* **17**, 553–563.

Goodarzi, A. A., Noon, A. T., Deckbar, D., Ziv, Y., Shiloh, Y., Löbrich, M. and Jeggo, P. A. (2008). ATM signaling facilitates repair of DNA double-strand breaks associated with heterochromatin. *Mol. Cell* **31**, 167–177.

Gosset, M., Berenbaum, F., Thirion, S. and Jacques, C. (2008). Primary culture and phenotyping of murine chondrocytes. *Nat. Protoc.* **3**, 1253–1260.

Guilak, F. (1995). Compression-induced changes in the shape and volume of the chondrocyte nucleus. *J. Biomech.* **28**, 1529–1541.

Journal of Cell Science • Accepted manuscript

Hong, X., Liu, W., Song, R., Shah, J. J., Feng, X., Tsang, C. K., Morgan, K. M., Bunting, S. F., Inuzuka, H., Zheng, X. F. S., et al. (2016). SOX9 is targeted for proteasomal degradation by the E3 ligase FBW7 in response to DNA damage. *Nucleic Acids Res.* **44**, 8855–8869.

Irianto, J., Swift, J., Martins, R. P., McPhail, G. D., Knight, M. M., Discher, D. E. and Lee, D. A. (2013). Osmotic challenge drives rapid and reversible chromatin condensation in chondrocytes. *Biophys. J.* **104**, 759–769.

Janssen, A., Colmenares, S. U. and Karpen, G. H. (2018). Heterochromatin: guardian of the genome. *Annu. Rev. Cell Dev. Biol.* **34**, 265–288.

Kirby, T. J. and Lammerding, J. (2018). Emerging views of the nucleus as a cellular mechanosensor. *Nat. Cell Biol.* **20**, 373–381.

Kobayashi, T. and Kronenberg, H. M. (2014). Overview of skeletal development - skeletal development and repair: methods and protocols. In (ed. Hilton, M. J.), pp. 3–12. Totowa, NJ: Humana Press.

Kozhemyakina, E., Lassar, A. B. and Zelzer, E. (2015). A pathway to bone: signaling molecules and transcription factors involved in chondrocyte development and maturation. *Development* **142**, pp. 817–831.

Le, H. Q., Ghatak, S., Yeung, C.-Y. C., Tellkamp, F., Günschmann, C., Dieterich, C., Yeroslaviz, A., Habermann, B., Pombo, A., Niessen, C. M., et al. (2016). Mechanical regulation of transcription controls Polycomb-mediated gene silencing during lineage commitment. *Nat. Cell Biol.* **18**, 864–875.

Lefebvre, V. (2019). Roles and regulation of SOX transcription factors in skeletogenesis. *Curr. Top. Dev. Biol.* **133**, 171–193.

Lefebvre, V. and Dvir-Ginzberg, M. (2017). SOX9 and the many facets of its regulation in the chondrocyte lineage. *Connect. Tissue Res.* **58**, 2–14.

Lefebvre, V., Angelozzi, M. and Haseeb, A. (2019). SOX9 in cartilage development and disease. *Curr. Opin. Cell Biol.* **61**, 39–47.

Li, G., Zheng, B., Meszaros, L. B., Vella, J. B., Usas, A., Matsumoto, T. and Huard, J. (2011). Identification and characterization of chondrogenic progenitor cells in the fascia of postnatal skeletal muscle. *J. Mol. Cell Biol.* **3**, 369–377.

Li, Y., Zhou, J., Yang, X., Jiang, Y. and Gui, J. (2016). Intermittent hydrostatic pressure maintains and enhances the chondrogenic differentiation of cartilage progenitor cells cultivated in alginate beads. *Dev. Growth Differ.* **58**, 180–193.

Journal of Cell Science • Accepted manuscript

Li, L., Newton, P. T., Bouderlique, T., Sejnohova, M., Zikmund, T., Kozhemyakina, E., Xie, M., Krivanek, J., Kaiser, J., Qian, H., et al. (2017). Superficial cells are self-renewing chondrocyte progenitors, which form the articular cartilage in juvenile mice. *FASEB J.* **31**, 1067–1084.

Liu, B., Wang, Z., Zhang, L., Ghosh, S., Zheng, H. and Zhou, Z. (2013). Depleting the methyltransferase Suv39h1 improves DNA repair and extends lifespan in a progeria mouse model. *Nat. Commun.* **4**, 1868.

Mazumder, A., Roopa, T., Basu, A., Mahadevan, L. and Shivashankar, G. V (2008). Dynamics of chromatin decondensation reveals the structural integrity of a mechanically prestressed nucleus. *Biophys. J.* **95**, 3028–3035.

Miller, K. M., Rog, O. and Cooper, J. P. (2006). Semi-conservative DNA replication through telomeres requires Taz1. *Nature* **440**, 824–828.

Miller, J. P., Yeh, N., Vidal, A. and Koff, A. (2007). Interweaving the cell cycle machinery with cell differentiation. *Cell Cycle* **6**, 2932–2938.

Miroshnikova, Y. A., Nava, M. M. and Wickström, S. A. (2017). Emerging roles of mechanical forces in chromatin regulation. *J. Cell Sci.* **130**, 2243 LP – 2250.

Miyanishi, K., Trindade, M. C. D., Lindsey, D. P., Beaupré, G. S., Carter, D. R., Goodman, S. B., Schurman, D. J. and Smith, R. L. (2006). Dose- and time-dependent effects of cyclic hydrostatic pressure on transforming growth factor-β3 induced chondrogenesis by adult human mesenchymal stem cells in vitro. *Tissue Eng.* **12**, 2253–2262.

Montagne, K., Onuma, Y., Ito, Y., Aiki, Y., Furukawa, K. S. and Ushida, T. (2017). High hydrostatic pressure induces pro-osteoarthritic changes in cartilage precursor cells: A transcriptome analysis. *PLoS One* **12**, e0183226.

Nava, M. M., Miroshnikova, Y. A., Biggs, L. C., Whitefield, D. B., Metge, F., Boucas, J., Vihinen, H., Jokitalo, E., Li, X., García Arcos, J. M., et al. (2020). Heterochromatin-driven nuclear softening protects the genome against mechanical stress-induced damage. *Cell* **181**, 800-817.e22.

Neumann, F. R. and Nurse, P. (2007). Nuclear size control in fission yeast. *J. Cell Biol.* **179**, 593–600.

Nirmalanandhan, V. S., Hurren, R., Cameron, W. D., Gronda, M., Shamas-Din, A., You, L., Minden, M. D., Rocheleau, J. V and Schimmer, A. D. (2015). Increased pressure alters plasma membrane dynamics and renders acute myeloid leukemia cells resistant to daunorubicin. *Haematologica* **100**, e406–e408.

Journal of Cell Science • Accepted manuscript

Ofek, G., Wiltz, D. C. and Athanasiou, K. A. (2009). Contribution of the cytoskeleton to the compressive properties and recovery behavior of single cells. *Biophys. J.* **97**, 1873–1882.

Panda, D. K., Miao, D., Lefebvre, V., Hendy, G. N. and Goltzman, D. (2001). The transcription factor SOX9 regulates cell cycle and differentiation genes in chondrocytic CFK2 cells. *J. Biol. Chem.* **276**, 41229–41236.

Pearson, C. E., Edamura, K. N. and Cleary, J. D. (2005). Repeat instability: mechanisms of dynamic mutations. *Nat. Rev. Genet.* **6**, 729–742.

Peters, A. H. F. M., Kubicek, S., Mechtler, K., O'Sullivan, R. J., Derijck, A. A. H. A., Perez-Burgos, L., Kohlmaier, A., Opravil, S., Tachibana, M., Shinkai, Y., et al. (2003). Partitioning and plasticity of repressive histone methylation states in mammalian chromatin. *Mol. Cell* **12**, 1577–1589.

Prystopiuk, V., Fels, B., Simon, C. S., Liashkovich, I., Pasrednik, D., Kronlage, C., Wedlich-Söldner, R., Oberleithner, H. and Fels, J. (2018). A two-phase response of endothelial cells to hydrostatic pressure. *J. Cell Sci.* **131**, jcs206920.

Schinagl, R. M., Gurskis, D., Chen, A. C. and Sah, R. L. (1997). Depth-dependent confined compression modulus of full-thickness bovine articular cartilage. *J. Orthop. Res.* **15**, 499–506.

Schindelin, J., Arganda-Carreras, I., Frise, E., Kaynig, V., Longair, M., Pietzsch, T., Preibisch, S., Rueden, C., Saalfeld, S., Schmid, B., et al. (2012). Fiji: an open-source platform for biological-image analysis. *Nat. Methods* **9**, 676–682.

Smart, D. J., Halicka, H. D., Schmuck, G., Traganos, F., Darzynkiewicz, Z. and Williams, G. M. (2008). Assessment of DNA double-strand breaks and gammaH2AX induced by the topoisomerase II poisons etoposide and mitoxantrone. *Mutat. Res.* **641**, 43–47.

Spaapen, F., van den Akker, G. G. H., Caron, M. M. J., Prickaerts, P., Rofel, C., Dahlmans, V. E. H., Surtel, D. A. M., Paulis, Y., Schweizer, F., Welting, T. J. M., et al. (2013). The immediate early gene product EGR1 and polycomb group proteins interact in epigenetic programming during chondrogenesis. *PLoS One* **8**, e58083–e58083.

Swift, J., Ivanovska, I. L., Buxboim, A., Harada, T., Dingal, P. C. D. P., Pinter, J., Pajerowski, J. D., Spinler, K. R., Shin, J.-W., Tewari, M., et al. (2013). Nuclear lamin-A scales with tissue stiffness and enhances matrix-directed differentiation. *Science.* **341**, 1240104.

Toledo, L. I., Murga, M., Zur, R., Soria, R., Rodriguez, A., Martinez, S., Oyarzabal, J., Pastor, J., Bischoff, J. R. and Fernandez-Capetillo, O. (2011). A cell-based screen

Journal of Cell Science • Accepted manuscript

identifies ATR inhibitors with synthetic lethal properties for cancer-associated mutations. *Nat. Struct. Mol. Biol.* **18**, 721–727.

Towbin, B. D., González-Aguilera, C., Sack, R., Gaidatzis, D., Kalck, V., Meister, P., Askjaer, P. and Gasser, S. M. (2012). Step-wise methylation of histone H3K9 positions heterochromatin at the nuclear periphery. *Cell* **150**, 934–947.

Tsang, K. Y. and Cheah, K. S. E. (2019). The extended chondrocyte lineage: implications for skeletal homeostasis and disorders. *Curr. Opin. Cell Biol.* **61**, 132–140.

Urban, J. P. G. (1994). The chondrocyte: a cell under pressure. *Rheumatology* **33**, 901–908.

Wuelling, M. and Vortkamp, A. (2011). Chondrocyte proliferation and differentiation. In *Endocrine Development*, pp. 1–11.

Yao, Y. and Wang, Y. (2013). ATDC5: An excellent in vitro model cell line for skeletal development. *J. Cell. Biochem.* **114**, 1223–1229.

Zhao, J., Bacolla, A., Wang, G. and Vasquez, K. M. (2010). Non-B DNA structure-induced genetic instability and evolution. *Cell. Mol. Life Sci.* **67**, 43–62.

Zhao, G., Wang, H., Xu, C., Wang, P., Chen, J., Wang, P., Sun, Z., Su, Y., Wang, Z., Han, L., et al. (2016). SIRT6 delays cellular senescence by promoting p27Kip1 ubiquitin-proteasome degradation. *Aging (Albany. NY).* **8**, 2308–2323.

Journal of Cell Science • Accepted manuscript

Figures

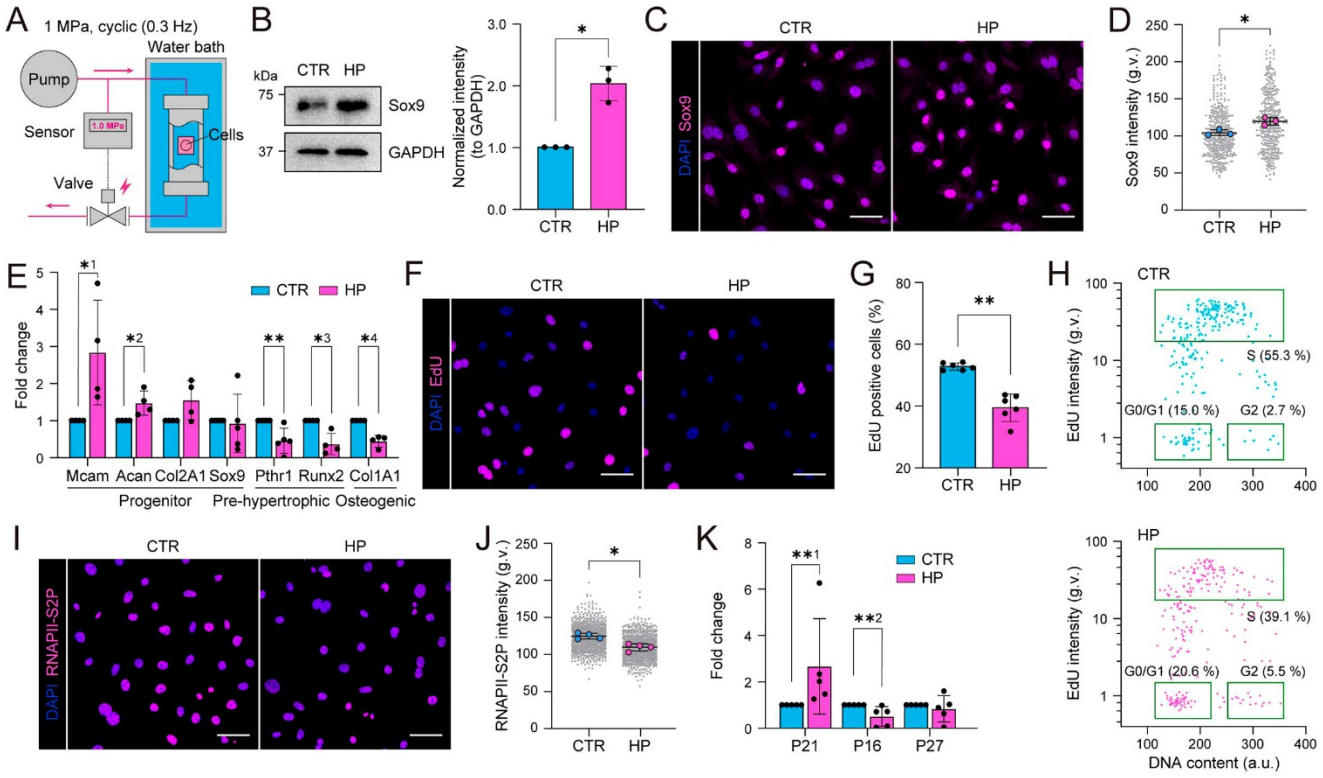


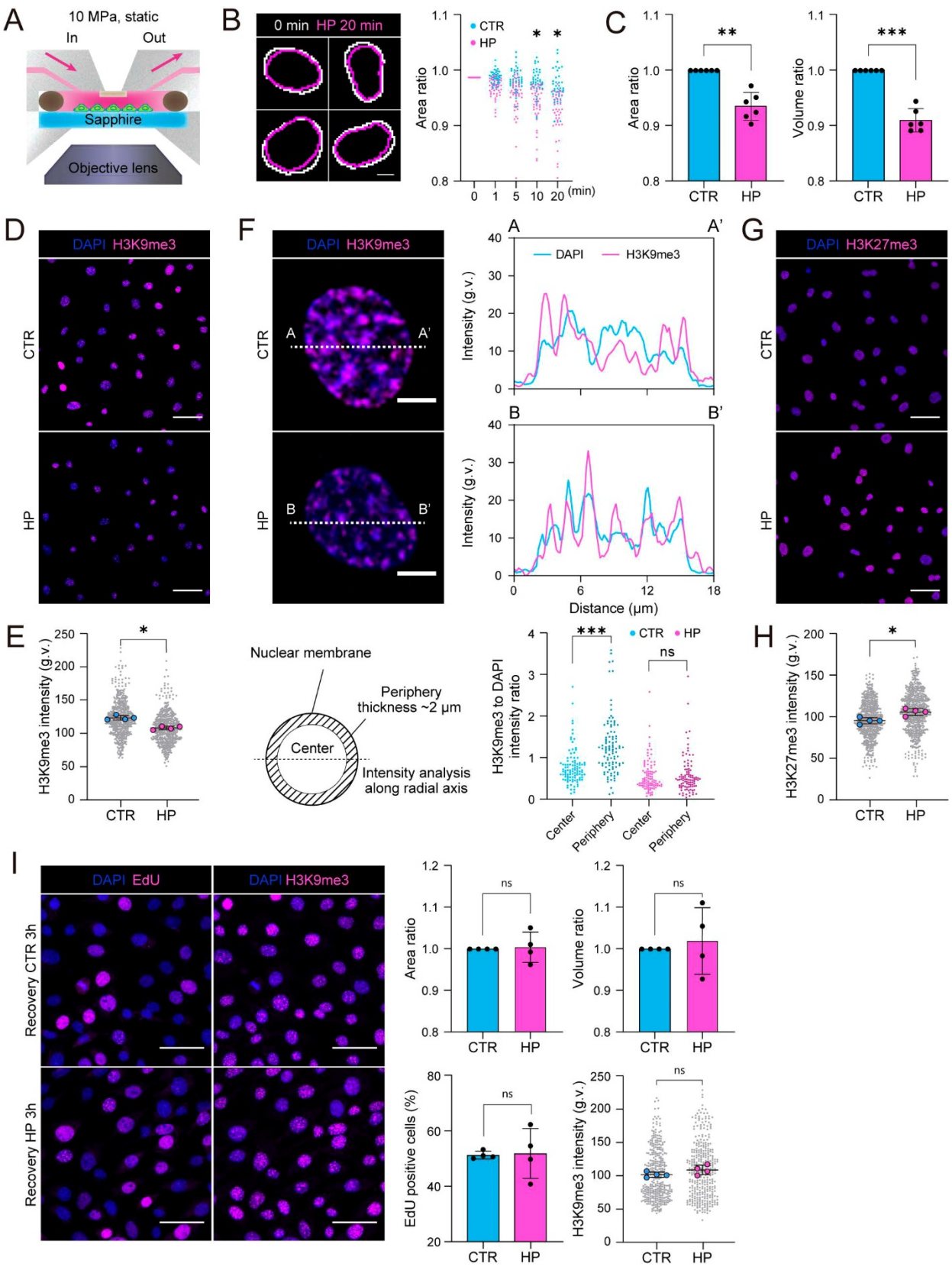
Figure 1. Hydrostatic pressure promotes a quiescent progenitor state of chondrocytes

(A) Schematic illustration of the experimental design for cyclic hydrostatic pressure (HP) application where a liquid chromatography pump is combined with a solenoid valve and a pressure sensor to induce cyclic HP with a 1 MPa threshold on cells in a water bath. **(B)** Representative western blots and quantification for Sox9 from cells exposed to cyclic HP for 6 h (n = 3 independent experiments; *p = 0.0217; one sample t-test). **(C)** Representative Sox9 (magenta) and nuclear (DAPI; blue) immunofluorescence images of cells exposed to cyclic HP for 6 h. **(D)** Quantification of immunofluorescence images in (C) shows increase in Sox9 intensity in response to HP (n = 3 independent experiments with >120 cells/condition/experiment; *p = 0.0217, Mann-Whitney). **(E)** qPCR analysis for chondrocyte progenitor marker Mcam, Acan, Col2A1, Sox9 and pre-hypertrophic and osteogenic differentiation markers Pthr1, Runx2, Col1A1 in HP loaded and corresponding control samples (n = 4 or 5 independent experiments; *^{1}p = 0.0286; *^{2}p = 0.0286; *^{3}p = 0.0286; *^{4}p = 0.0286; **p = 0.0079, Mann-Whitney). **(F)** Representative EdU (magenta) and nuclear (DAPI; blue) images of cells exposed to cyclic HP for 6 h. **(G)** Quantification of images in (F) shows a decrease in EdU-positive cells (%) in response to HP (n = 6 independent experiments with >255 cells/condition/experiment; **p = 0.0022, Mann-Whitney). **(H)** Scatter plots of EdU intensity versus DNA content (from DAPI stain) in control (top) and HP-loaded samples (bottom) show an increase in G0/G1 phase population and a corresponding decrease in S

Journal of Cell Science • Accepted manuscript

phase population upon HP (n = 263 cells/condition). **(I)** Representative RNAPII-S2P (magenta) and nuclear (DAPI; blue) immunofluorescence images of cells exposed to cyclic HP for 6 h. **(J)** Quantification of images in (I) shows a decrease in RNAPII-S2P intensity in cells exposed to HP (n = 4 independent experiments with >165 cells/condition/experiment; *p = 0.0286, Mann-Whitney). **(K)** qPCR analysis for quiescence and senescent markers in HP loaded and corresponding control samples (n = 5 independent experiments; $**^{1}$p = 0.0079, $**^{2}$p = 0.0079, Mann-Whitney). All bar graphs show mean ±SD, scale bars represent 50 µm, g.v. = gray values.

Journal of Cell Science • Accepted manuscript

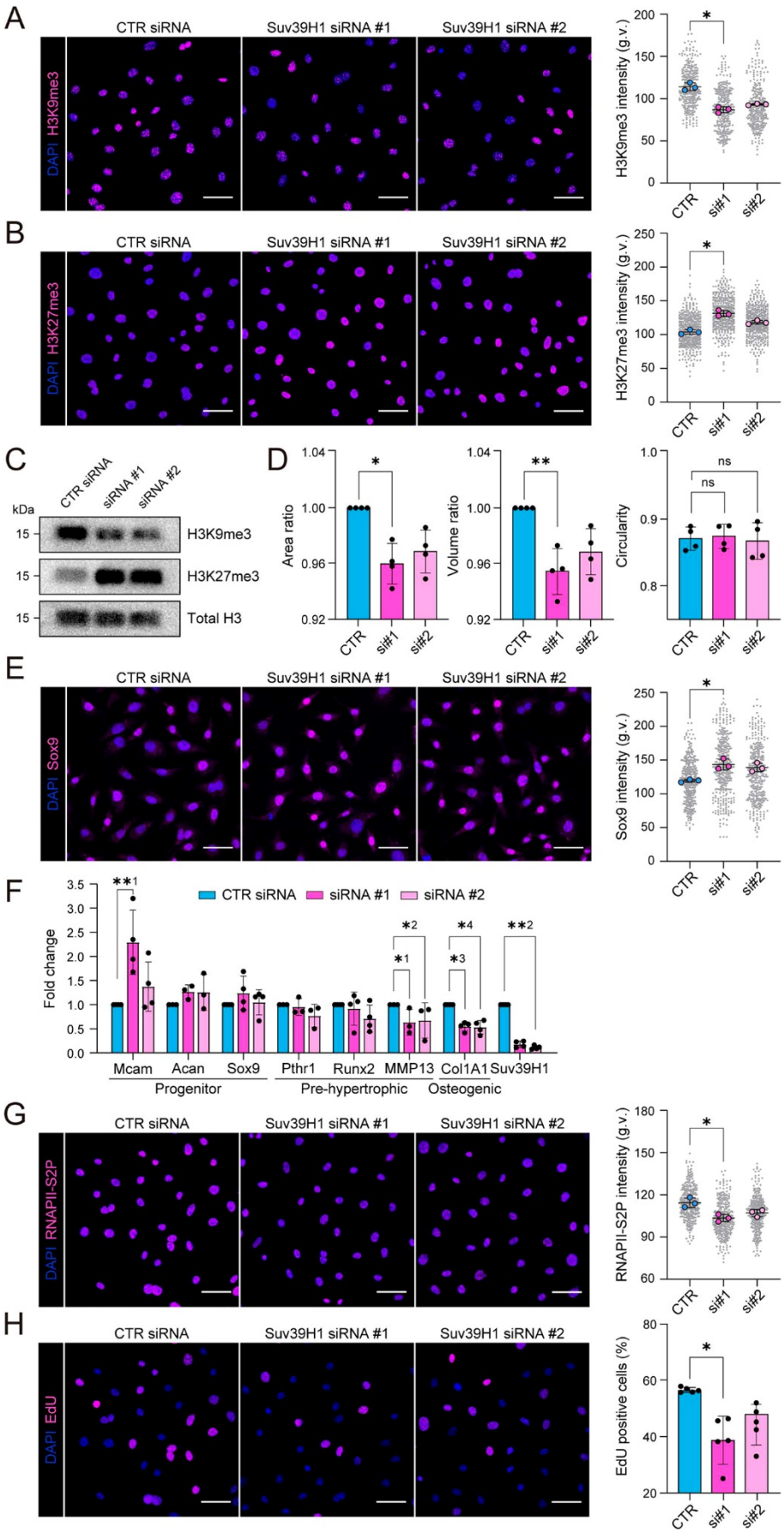


Journal of Cell Science • Accepted manuscript

Figure 2. Hydrostatic pressure triggers nuclear shrinkage and heterochromatin remodeling

(A) Schematic illustration of the experimental design for live-imaging under HP. Cells seeded on a sapphire glass were treated with Hoechst 33342 to visualize nuclei and loaded under constant HP in a stainless steel chamber mounted on an epifluorescence microscope. **(B)** Representative nuclear outlines (left) and time-resolved quantification of nuclear area ratio (right) in the absence of loading (cyan) and upon HP (magenta) (n = 42 cells/condition; *p < 0.001, Two-way ANOVA/Sidak's; Scale bar 5 µm). **(C)** Quantification of immunofluorescence images shows a decrease in nuclear area and volume in response to cyclic HP, without significant change in nuclear shape (n = 6 independent experiments with >250 cells/condition/experiment; **p = 0.0015, ***p = 0.0001, One sample t-test). **(D)** Representative H3K9me3 (magenta) and nuclear (DAPI; blue) images of cells exposed to cyclic HP for 6 h. Scale bars 50 µm. **(E)** Quantification of images in (D) shows a decrease in H3K9me3 level in response to HP (n = 4 independent experiments with >130 cells/condition/experiment; *p = 0.0286, Mann-Whitney). **(F)** Quantification of H3K9me3 levels within the nuclear periphery and center using linescan analyses (upper panels) and subsequent separation of nuclei into two areas of interest (lower panels). Intensity ratio (H3K9me3/DAPI) within central and peripheral areas of interest shows decreased H3K9me3 in particular at the nuclear periphery upon HP (n = 100 cells/condition; ***p < 0.0001, Friedman/Dunn's). Scale bars 5 µm. **(G)** Representative H3K27me3 (magenta) and nuclear (DAPI; blue) images of cells exposed to cyclic HP for 6 h. Scale bars 50 µm. **(H)** Quantification of images in (G) shows increased H3K27me3 levels by HP (n = 4 independent experiments with >115 cells/condition/experiment; *p = 0.0286, Mann-Whitney). **(I)** Representative EdU and H3K9me3 (magenta) and nuclear (DAPI; blue) images of chondrocytes exposed to cyclic HP for 6 h followed by 3 h incubation. Intensity and nuclear size quantifications in bar graphs show no significant differences (n = 4 independent experiments with >80 cells/condition/experiment; p > 0.05 for all analysis, ns = not significant, Mann-Whitney). Scale bars 50 µm. All bar graphs show mean ±SD, g.v. = gray values.

Journal of Cell Science • Accepted manuscript

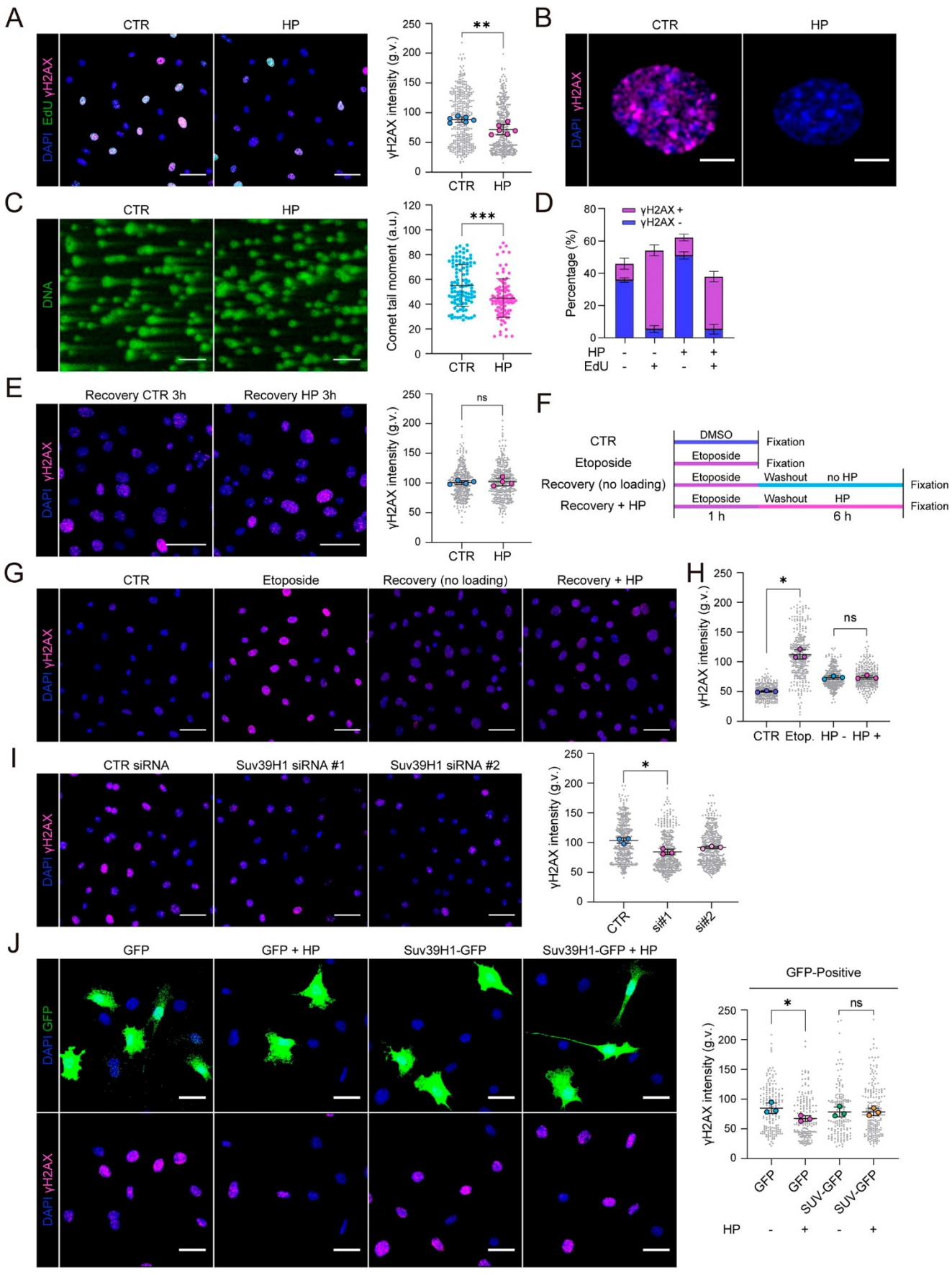


Journal of Cell Science • Accepted manuscript

Figure 3. H3K9me3 heterochromatin regulates chondrocyte quiescence and identity

(A) Representative H3K9me3 (magenta) and nuclear (DAPI; blue) immunofluorescence images of cells upon siRNA knockdown of Suv39H1 (left panel). Right panel shows quantification of H3K9me3 intensity (n = 3 independent experiments with >100 cells/condition/experiment; *p = 0.0286, Friedman/Dunn's). **(B)** Representative H3K27me3 immunofluorescence images upon Suv39H1 knockdown and intensity quantification (n = 3 independent experiments with >110 cells/condition/experiment; *p = 0.0286, Friedman/Dunn's). **(C)** Representative western blots for histone modification H3K9me3 and H3K27me3 upon Suv39H1 knockdown. **(D)** Quantification of nuclear area, volume, and circularity (n = 4 independent experiments with >110 cells/condition/experiment; *p = 0.0228, **p = 0.0094, ns = not significant, Friedman/Dunn's). **(E)** Representative Sox9 immunofluorescence images and intensity quantifications of in control and Suv39H1 knockdown cells (n = 3 independent experiments with >110 cells/condition/experiment; *p = 0.0286, Friedman/Dunn's). **(F)** qPCR analysis for chondrocyte progenitor marker Mcam, Acan, Sox9, and pre-hypertrophic and osteogenic differentiation markers Pthr1, Runx2, MMP13, Col1A1 in Suv39H1 knockdown samples (n = 3 or 4 independent experiments; $*^{1}p$ = 0.0487, $*^{2}p$ = 0.0338, $*^{3}p$ = 0.0166, $*^{4}p$ = 0.0166, $**^{1}p$ = 0.0095, $**^{2}p$ = 0.0038, Kruskal-Wallis/Dunn's). **(G-H)** Representative RNAPII-S2p and EdU immunofluorescence images and intensity quantifications of in control and Suv39H1 knockdown cells (n = 3 (RNAPII-S2P) or 5 (EdU) independent experiments with >110 cells/condition/experiment; *p = 0.0286 (RNAPII-S2p); *p = 0.0228 (EdU), Friedman/Dunn's). All bar graphs show mean ±SD. All scale bars represent 50 µm, g.v. = gray values.

Journal of Cell Science • Accepted manuscript



Journal of Cell Science • Accepted manuscript

Figure 4. Hydrostatic pressure-controlled chondrocyte quiescence prevents replicative stress

(A) Representative EdU (green)/γH2AX (magenta) immunofluorescence images of cells exposed to cyclic HP for 6 h and intensity quantification of γH2AX shows increased levels of γH2AX upon HP (n = 6 independent experiments with >250 cells/condition/experiment; **p = 0.0050, Paired ratio t-test). Scale bars 50 µm. **(B)** Representative immunofluorescence image showing pan-nuclear staining pattern of γH2AX in CTR and attenuated signal in HP. Scale bars 5 µm. **(C)** Representative images of alkaline comet assays from cells exposed to cyclic HP for 6 h and quantification of comet tails. Note decreased presence of comet tails in cells exposed to HP (n = >100 cells/condition; ***p = 0.0001, Mann–Whitney). Scale bars 50 µm. **(D)** Quantification of the relationship of EdU/γH2AX in single cells. Note that EdU-negative cells are predominantly γH2AX-negative, whereas EdU-positive cells are predominantly also γH2AX-positive both in control cells and cells exposed to HP (n = 3 independent experiments with >180 cells/condition/experiment). **(E)** Representative γH2AX (magenta) and nuclear (DAPI; blue) images of chondrocytes exposed to cyclic HP for 6 h followed by 3 h incubation (n = 4 independent experiments with >80 cells/condition/experiment; ns = not significant, Mann-Whitney). Scale bars 50 µm. **(F)** Schematics of the recovery experiment with HP loading after DNA damage induction by pulse treatment of Etoposide (10 µM, 1 h). **(G)** Representative γH2AX immunofluorescence images of cells obtained in the recovery experiment (F). Scale bars 50 µm. **(H)** Quantification of immunofluorescence images in (G) shows increased γH2AX signals after Etoposide pulse but no significant effect of HP loading on removal of γH2AX (n = 3 independent experiments with >120 cells/condition/experiment; *p = 0.0134, Friedman/Dunn's). **(I)** Representative γH2AX immunofluorescence images from cells depleted of Suv39H1 and intensity quantification (n = 3 independent experiments with >110 cells/condition/experiment; *p = 0.0286, Friedman/Dunn's). Scale bars 50 µm. **(J)** Representative γH2AX immunofluorescence images and quantification from chondrocytes expressing GFP (control) and Suv39H1-IRES-EGFP exposed to cyclic HP for 6 h (n = 3 independent experiments with >50 cells/condition/experiment; *p = 0.0266, ns = not significant, Friedman/Dunn's). Scale bars 20 µm. All bar graphs show mean ±SD, a.u.=arbitrary units, g.v. = gray values.

Journal of Cell Science • Accepted manuscript

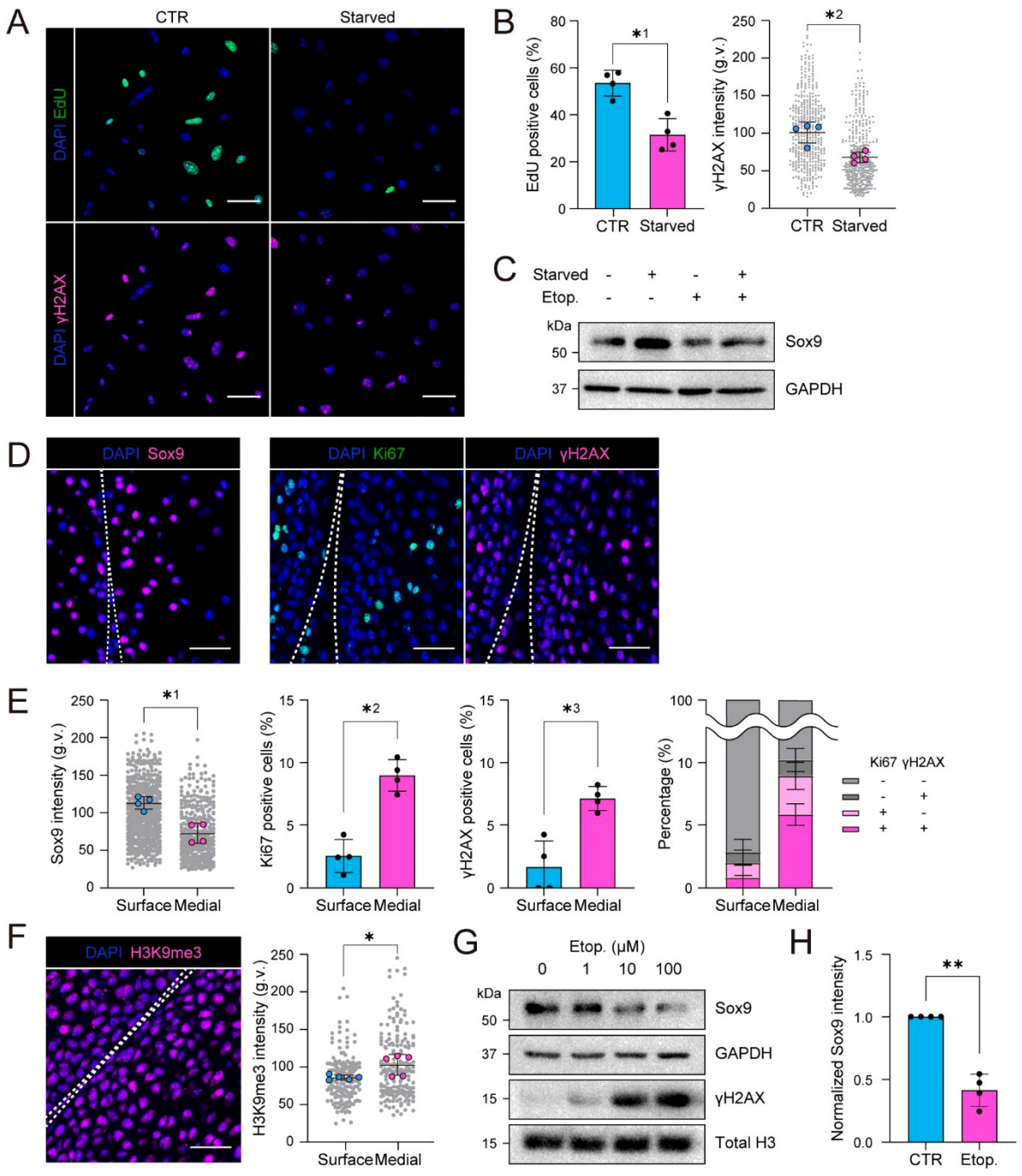


Figure 5. Loss of quiescence induces replicative stress to promote loss of chondrocyte identity (progenitor state)

(A) Representative EdU/γH2AX chemiluminescence/immunofluorescence images of cells after 24 h serum starvation. Scale bars 50 µm. **(B)** Quantification of immunofluorescence images in (A) shows a decrease in EdU incorporation (top) and γH2AX intensity (bottom) after starvation (n = 4 independent experiments with >100 cells/condition/experiment; $*^1p$ = 0.0286, $*^2p$ = 0.0286, Mann-Whitney). **(C)** Representative western blots for Sox9 from cells starved for 24 h followed by Etoposide treatment (10 µM, 6 h). **(D)** Representative Sox9, Ki67 and γH2AX immunofluorescence images of articular cartilage in vivo from postnatal day 2 (P2) mouse cartilage. Note that Ki67-positive cells are predominantly γH2AX-positive in the

Journal of Cell Science • Accepted manuscript

medial zone. Scale bars 30 μm. **(E)** Quantification for Sox9 (left), Ki67 (middle) and γH2AX intensity (right) at surface and medial zones (n = 4 mice with >90 cells/zone/mouse; $*^1$p = 0.0286, $*^2$p = 0.0286, $*^3$p = 0.0286, Mann-Whitney). Distance ranges of 0-30 μm and 30-60 μm from cartilage surface are defined as surface and medial, respectively. Right panel shows the relationship of Ki67/γH2AX in single cells. Note that Ki67-positive cells are predominantly γH2AX-positive in the medial zone (n = 3 independent experiments with >152 cells/zone/condition). **(F)** Representative immunofluorescence image and quantification of H3K9me3 in articular cartilage in vivo from P2 mice (n = 5 mice with >90 cells/zone/mouse; *p = 0.0317, Mann-Whitney). Scale bars 30 μm. **(G)** Representative western blots for Sox9 and γH2AX for samples treated with indicated concentrations of Etoposide for 6 h. Note dose-dependent decrease in Sox9. **(H)** Quantification for Sox9 intensity in western blots for samples exposed to Etoposide treatment (10 μM, 6 h) (n = 4 independent experiments; **p = 0.0028, One sample t-test). g.v. =gray values.

Journal of Cell Science • Accepted manuscript

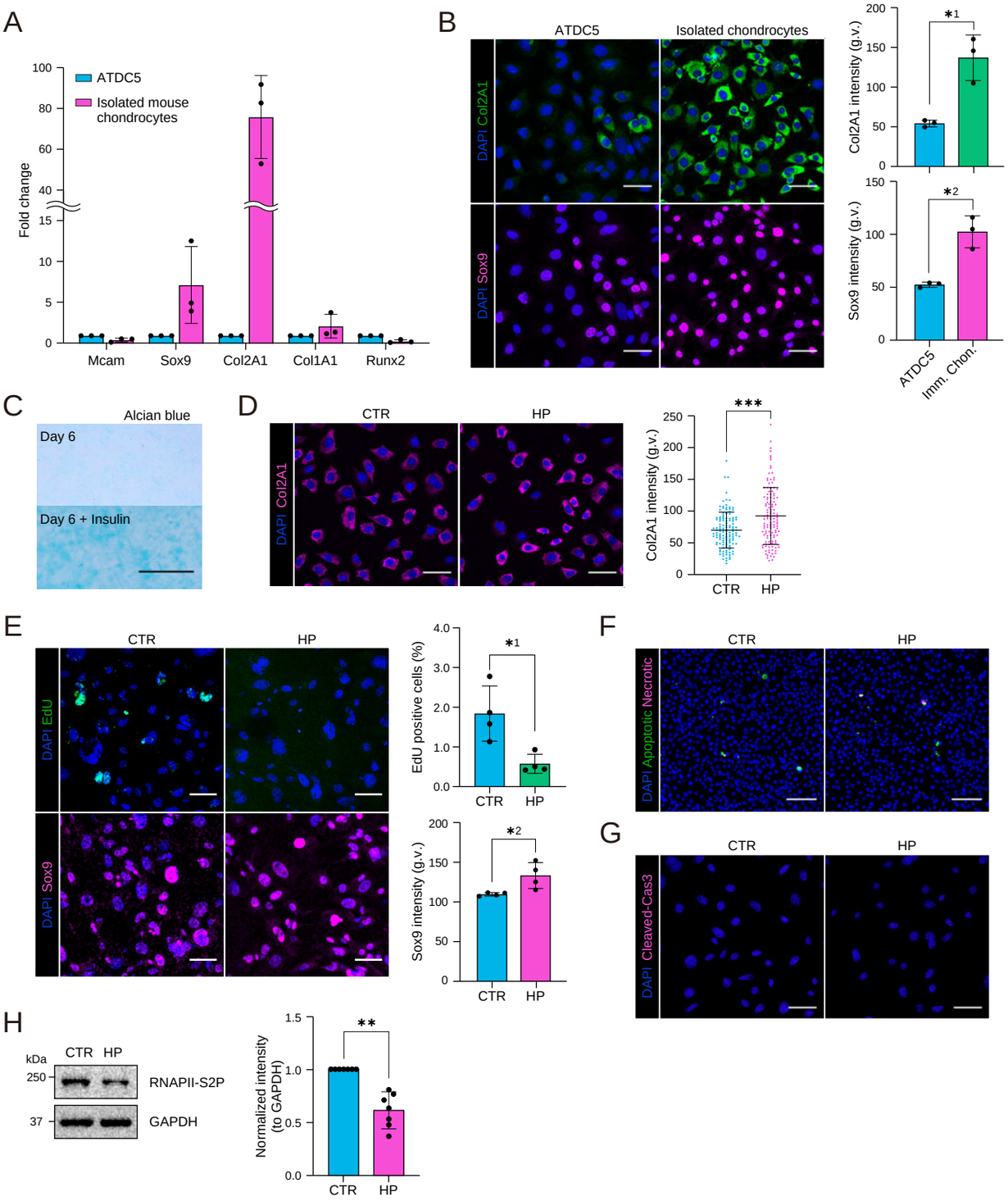


Figure S1.
(A) qPCR of chondrocyte key identity gene expression for ATDC5 and isolated mouse chondrocytes (n = 3 independent experiments). (B) Representative Col2A1 (green), Sox9 (magenta) and DAPI (blue) images of ATDC5 and isolated mouse chondrocytes (n = 3 independent experiments with >155 cells/condition/experiment; ^{*1}p = 0.0280, ^{*2}p = 0.0326, Paired t-test). (C) Alcian blue staining for insulin-stimulated mouse chondrocytes. Scale bar 100 µm. (D) Representative Col2A1 (magenta) and nuclear (DAPI; blue) images of chondrocytes exposed to cyclic HP for 6 h (n >110 cells/condition; ***p < 0.0001, Mann-Whitney). Scale bar 50 µm. (E) Representative EdU (green), Sox9 (magenta) and nuclear (DAPI; blue) images of non-immortalized chondrocytes exposed to cyclic HP for 6 h (n = 4 independent experiments with >115 cells/condition/experiment; ^{*1}p = 0.0286, ^{*2}p = 0.0286, Mann-Whitney. Scale bar 50 µm. (F) Representative FITC-Annexin V (green), Ethidium Homodimer III (magenta) and DAPI (blue) images of cells exposed to cyclic HP. Scale bar 300 µm. (G) Representative Cleaved Caspase-3 (magenta) and DAPI (blue) images of cells exposed to cyclic HP for 6 h. Scale bar 50 µm. (H) Representative western blots and quantification for RNAPII-S2P for samples exposed to cyclic HP for 6 h (n = 7 independent experiments; **p=0.0012, One sample t-test). All bar graphs show mean ±SD, g.v. = gray values.

Journal of Cell Science • Supplementary information

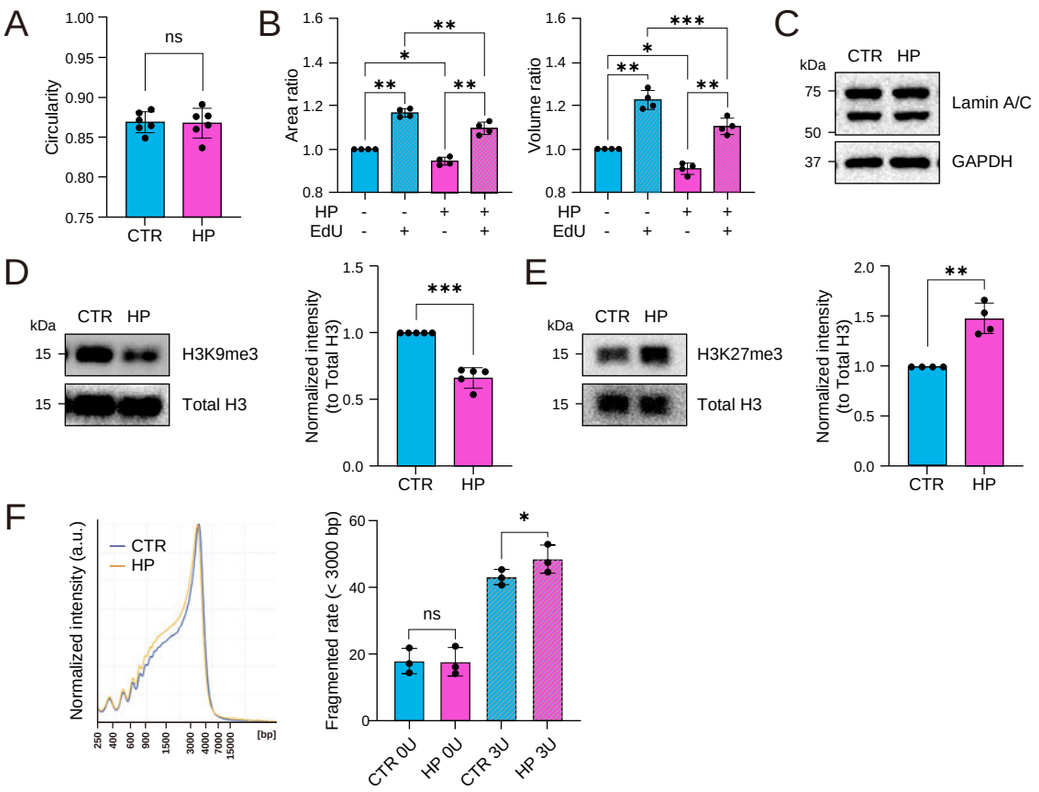


Figure S2.
(A) Quantification of nuclear morphology from DAPI-stained cells (cyclic HP, 6 h) shows no significant change in nucleus circularity (n = 6 independent experiments with >250 cells/condition/experiment). (B) Nuclear area (left) and volume (right) were analyzed for chondrocytes exposed to cyclic HP for 6 h and stained/labeled with DAPI and EdU. Cells were classified into EdU positive and negative groups based on two separated intensity distribution and then subjected to nuclear size analysis (n = 4 independent experiments with >105 cells/condition/experiment; *p < 0.05/**p < 0.01/***p < 0.001, RM one-way ANOVA). (C) Representative western blots and quantification for Lamin A/C from cells exposed to cyclic HP for 6 h. (D, E) Representative western blots and quantification for H3K9me3 and H3K27me3 from cells exposed to cyclic HP for 6 h (n = 5 and 4 independent experiments; ***p = 0.0007 (H3K9me3); **p = 0.0058 (H3K27me3), one sample t-test). (F) Results of Micrococcal chromatin fragmentation assay after HP-loading (left and center panel) (n = 3 independent experiments; *p = 0.0419, ns = not significant, Paired t-test). All bar graphs show mean ±SD.

Journal of Cell Science • Supplementary information

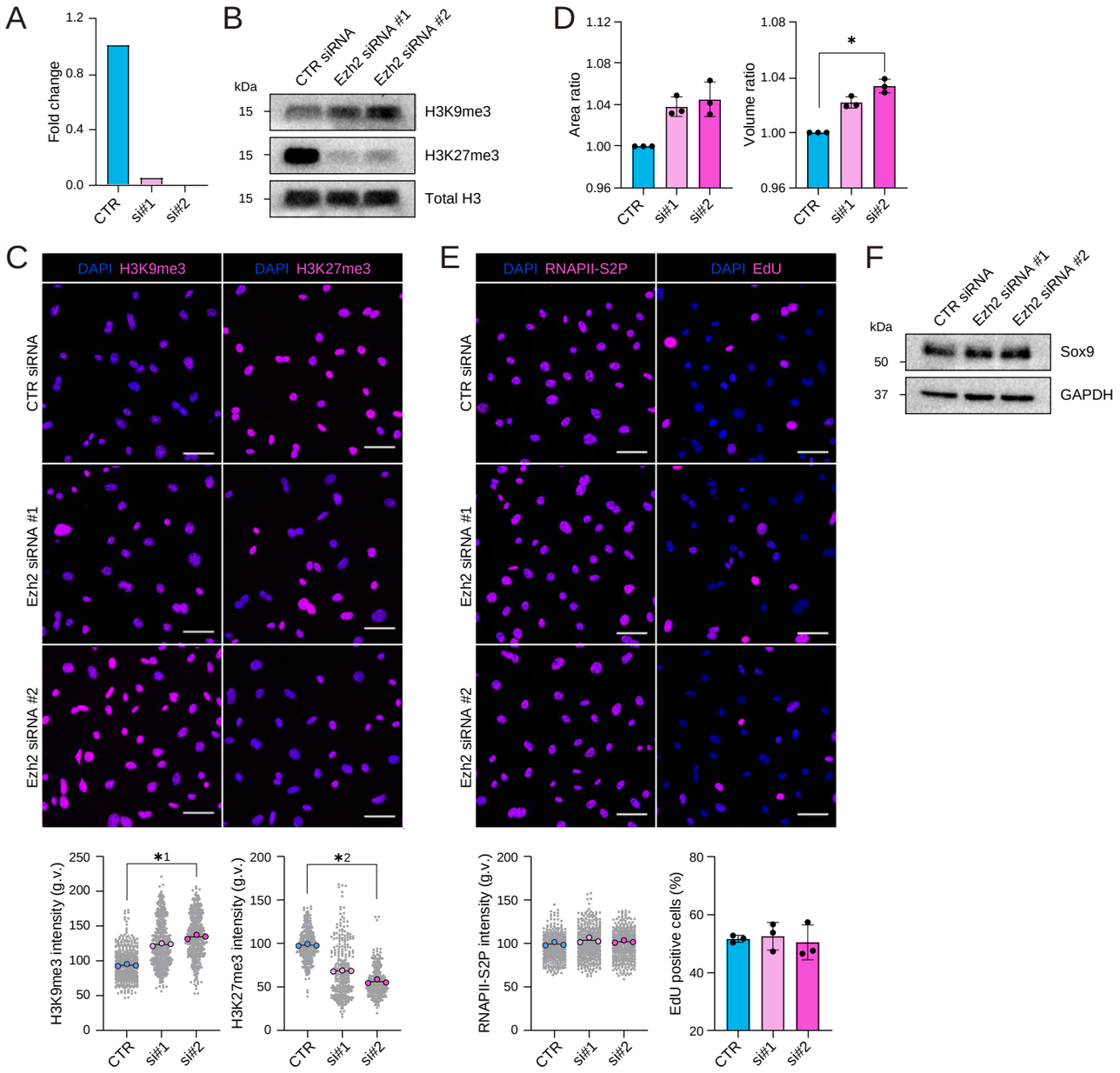


Figure S3.
(A) qPCR for Ezh2 upon siRNA knockdown. (B) Representative western blots for H3K9me3 and H3K27me3 upon Ezh2 knockdown. (C) Representative H3K9me3 and H3K27me3 immunofluorescence images and intensity quantification upon Ezh2 knockdown (n = 3 independent experiments with >105 cells/condition/experiment; $^{*1}p = 0.0286$, $^{*2}p = 0.0286$, Mann-Whitney). (D) Quantification of immunofluorescence images from DAPI-stained cells shows increase in nuclear area and volume in response to HP (n = 3 independent experiments with >105 cells/condition/experiment; *p = 0.0286, One sample t-test). (E) Representative H3K9me3, H3K27me3, RNAPII-S2P and EdU immunofluorescence/chemiluminescence images and intensity quantification upon Ezh2 knockdown (n = 3 independent experiments with >110 cells/condition/experiment). (F) Representative western blots for Sox9 upon Ezh2 knockdown. All bar graphs show mean ±SD, scale bars 50 µm, g.v. = gray values.

Journal of Cell Science • Supplementary information

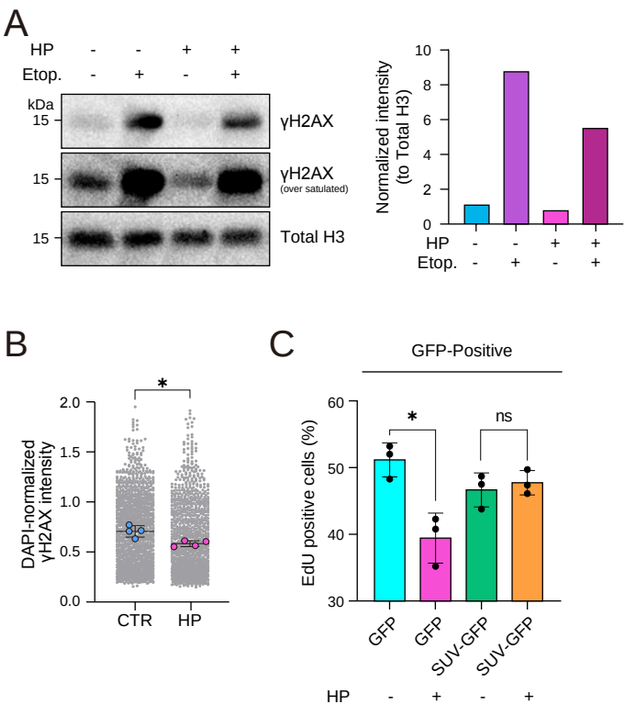


Figure S4.
(A) Representative western blots for γH2AX from chondrocytes exposed to cyclic HP for 6 h with and without etoposide treatment (10 μM). (B) Intensity quantification for γH2AX staining in Fig. 4A by DAPI-normalization shows decreased level of γH2AX upon HP (n = 4 independent experiments with >250 cells/condition/experiment; *p = 0.0286, Mann-Whitney). (C) Quantification of EdU positive cells in chondrocytes expressing GFP (control) and Suv39H1-IRES-EGFP exposed to cyclic HP for 6 h (n = 3 independent experiments with >50 cells/condition/experiment; *p = 0.0266, ns = not significant, Friedman/Dunn's).

Journal of Cell Science • Supplementary information

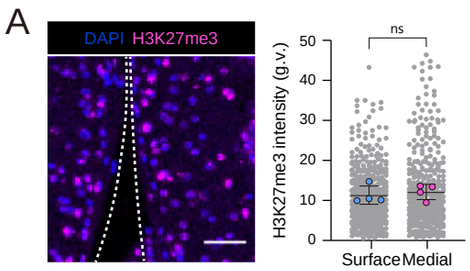
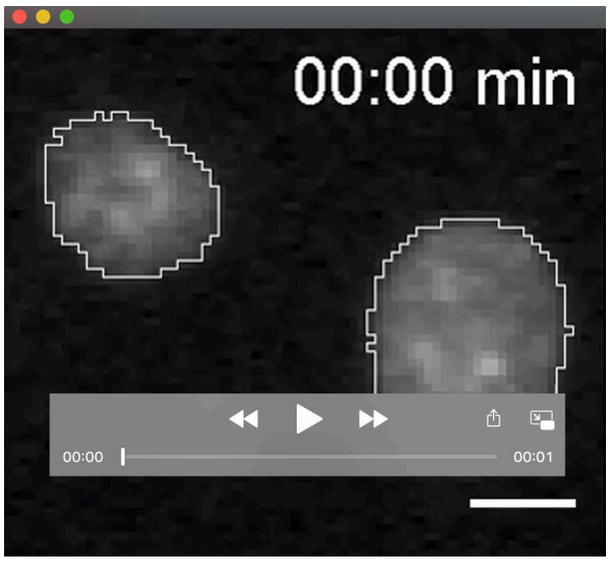


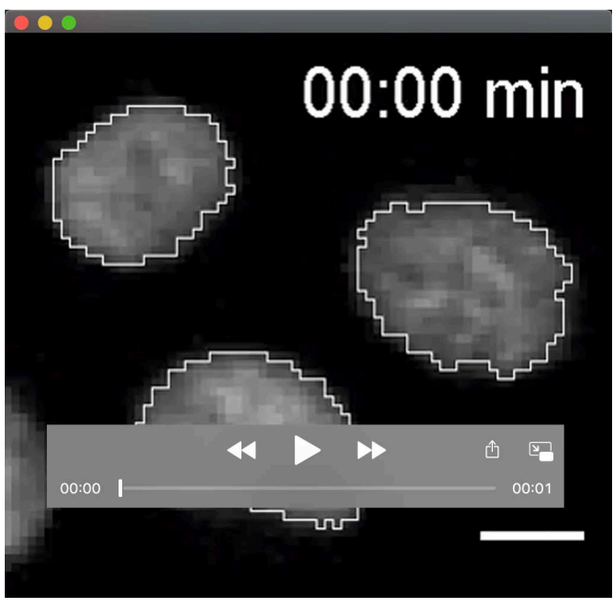
Figure S5.

(A) Representative H3K27me3 immunofluorescence image of articular cartilage from postnatal day 2 (P2) mouse, and quantification of intensity at surface and medial zones (n = 4 mice with >50 cells/zone/mouse; ns = not significant, Mann-Whitney). Scale bar 30 μm, g.v. =,gray values.

Journal of Cell Science • Supplementary information



Movie 1. Real time imaging of ATDC5 cells without hydrostatic pressure Representative movie of ATDC cells without hydrostatic pressure. Initial nuclear outline is indicated in a cyan line and the nuclear outline in each frame is traced in magenta. Frame rate 30 sec/frame. Scale bar 20 μm.



Movie 2. Real time imaging of ATDC5 cells under hydrostatic pressure Representative movie of ATDC cells exposed to 10 MPa hydrostatic pressure. Initial nuclear outline is indicated in a cyan line and the nuclear outline in each frame is traced in magenta. Frame rate 30 sec/frame. Scale bar 20 μm.

Journal of Cell Science • Supplementary information

Table S1

Gene	Forward	Reverse
Tubb	GAGCAGTTCACAGCCATGTT	CCAGGTCATTCATGTTGCTCTC
Actb	TCAAGATCATTGCTCCTCCTG	TACTTCTGCTTGCTGATCCAC
Col2A1	ACGAAGCGGCTGGCAACCTCA	CCCTCGGCCCTCATCTCTACATCA
Col1A1	GGCTGTGTGCGATGACGTGCAA	TCCGGGCAGAAAGCACAGCACT
Acan1	GTGAGGACCTGGTAGTGCGAGTGA	GAGCCTGGGCGATAGTGGAATATA
Sox9	CGATTACAAGTACCAGCCCCGG	TGCAGCGCCTTGAAGATAGCAT
Suv39H1	TTGGCACCCACTGGAGGCTGTT	TGCCCAGCTTTCAGTCGCACCT
Runx2	ACCCAGCCACCTTTACCTAC	TATGGAGTGCTGCTGGTCTG
Ezh2	TCACGTGTGGAGCTGCTGACCA	AAGATGCCCCAGCCTGCCACAT
Mcam	TGCCATGTGGACGCTCGGGAAA	TCACCGTTGCTGCCCTGAAGGA
P21	TGAGCAGTTGCGCCGTGATTGC	AACGCGCTCCCAGACGAAGTTG
P16	TGCAATCACGGGAGGGAGCAGA	ATTATTCCCTTCGCGGCCGCCT
P27	TCCTGACCAGCGGCTGCATCAT	GCGCCGTAGATCACCGTGTTCT
Pthr1	ACCTTGGCCAACACTGGGTGCT	AGCTTAGTGGCAAGCACCCGGA
MMP13	AGGCGATGAAGACCCCAACCCT	AGGGTGCAGGCGCCAGAAGAAT

Journal of Cell Science • Supplementary information